



# Industrial SO<sub>2</sub> emission monitoring through a portable multichannel gas analyzer with an optimized retrieval algorithm

Youwen Sun<sup>1,\*</sup>, Cheng Liu<sup>2,3,1,\*</sup>, Pinhua Xie<sup>1,2</sup>, Andreas Hartl<sup>4</sup>, Kalok Chan<sup>5</sup>, Yuan Tian<sup>1</sup>, Wei Wang<sup>1</sup>, Min Qin<sup>1</sup>, Jianguo Liu<sup>1,2</sup>, and Wenqing Liu<sup>1,2</sup>

<sup>1</sup>Key Lab of Environmental Optics & Technology, Anhui Institute of Optics and Fine Mechanics, Chinese Academy of Sciences, Hefei 230031, China

<sup>2</sup>School of Earth and Space Sciences, University of Science and Technology of China, Hefei 230026, China

<sup>3</sup>Center for Excellence in Urban Atmospheric Environment, Institute of Urban Environment, Chinese Academy of Sciences, Xiamen 361021, China

<sup>4</sup>School of Energy and Environment, City University of Hong Kong, Hong Kong

<sup>5</sup>Meteorological Institute, Ludwig-Maximilians-Universität München, Munich, Germany

\*These authors contributed equally to this work.

Correspondence to: Cheng Liu (chliu81@ustc.edu.cn) and Youwen Sun (ywsun@aiofm.ac.cn)

Received: 21 July 2015 – Published in Atmos. Meas. Tech. Discuss.: 17 December 2015

Revised: 9 March 2016 – Accepted: 13 March 2016 – Published: 21 March 2016

**Abstract.** SO<sub>2</sub> variability over a large concentration range and interferences from other gases have been major limitations in industrial SO<sub>2</sub> emission monitoring. This study demonstrates accurate industrial SO<sub>2</sub> emission monitoring through a portable multichannel gas analyzer with an optimized retrieval algorithm. The proposed analyzer features a large dynamic measurement range and correction of interferences from other coexisting infrared absorbers such as NO, CO, CO<sub>2</sub>, NO<sub>2</sub>, CH<sub>4</sub>, HC, N<sub>2</sub>O, and H<sub>2</sub>O. The multichannel gas analyzer measures 11 different wavelength channels simultaneously to correct several major problems of an infrared gas analyzer including system drift, conflict of sensitivity, interferences among different infrared absorbers, and limitation of measurement range. The optimized algorithm uses a third polynomial instead of a constant factor to quantify gas-to-gas interference. Measurement results show good performance in the linear and nonlinear ranges, thereby solving the problem that the conventional interference correction is restricted by the linearity of the intended and interfering channels. The results imply that the measurement range of the developed multichannel analyzer can be extended to the nonlinear absorption region. The measurement range and accuracy are evaluated through experimental laboratory calibration. Excellent agreement was achieved, with a Pearson correlation coefficient ( $r^2$ ) of 0.99977 with a measurement

range from approximately 5 to 10 000 ppmv and a measurement error of less than 2%. The instrument was also deployed for field measurement. Emissions from three different factories were measured. The emissions of these factories have been characterized by different coexisting infrared absorbers, covering a wide range of concentration levels. We compared our measurements with commercial SO<sub>2</sub> analyzers. Overall, good agreement was achieved.

## 1 Introduction

High-accuracy SO<sub>2</sub> emission monitoring is in demand for industrial process identification and pollution emission regulation. Industrial SO<sub>2</sub> emissions often vary over a wide range during different production processes (Chan and Yao, 2008; Terje, 1996; Zu, 2002; Liu, et al., 2011). For example, SO<sub>2</sub> emissions from a copper smelting plant are of the order of parts per million by volume (ppmv) or even less when the smelting period is nearly finished, but SO<sub>2</sub> emissions can be up to several thousands of ppmv or even higher during the smelting period. SO<sub>2</sub> emissions from industrial desulfurization processes (a chemical reaction process performed to reduce SO<sub>2</sub> emissions) are usually higher than 600 ppmv during the process, but lower than 200 ppmv otherwise (EPER,

2004; European Commission, 2007; Evans et al., 2009). Accurately measuring the variation in SO<sub>2</sub> concentrations in such a wide range with a single absorption band analyzer is impossible because of the conflict of sensitivity and limitation of measurement range (Andre et al., 1985; Dirk et al., 2009). Furthermore, stack emissions also consist of many other infrared-absorbing gases, such as NO, CO, CO<sub>2</sub>, NO<sub>2</sub>, N<sub>2</sub>O, HC, CH<sub>4</sub>, and H<sub>2</sub>O. All these gases may interfere with one another (Andre et al., 1985; Dirk et al., 2009). Cross-interferences have to be corrected to measure SO<sub>2</sub> emissions with high accuracy. In general, a commercial multi-gas analyzer (e.g., Model 60i made by Thermo Fisher Scientific or Li-7500 made by Li-Cor) specifies a particular application where the intended and interfering channels lie within linear ranges. Thus, cross-interference can be corrected through the conventional look-up table (consisting of various constant factors quantifying gas-to-gas interferences) approach (Herget et al., 1976; Jacob and Roy, 2012; Dirk et al., 2009; Harold et al., 1993). In this case, SO<sub>2</sub> concentrations within a certain linear range can be well resolved. However, the conventional interference correction introduces large uncertainty because of nonlinear absorption when the intended or interfering gases concentration lies beyond a threshold (Sun et al., 2013). In cases where the conventional correction of cross-interferences is impossible, one has to resort to other methods. For example, one can expand the linear range to higher concentrations by reducing the optical path length or selecting a relatively weak absorption waveband. However, both approaches have considerable disadvantages (Mark et al., 1983; Mauri et al., 2001). Reducing the optical path length influences the entire measurement system. The sensitivity and measurement range of other gases also deteriorate. Selecting a relatively weaker absorption waveband for a certain gas reduces the sensitivity to this gas for all applications (Lambrecht, 2005; Gary, 2002). Sun et al. (2013) proposed a new cross-interference correction technique that works well even when nonlinear absorption occurs (Sun et al., 2013). Consequently, the measurement range of a multichannel analyzer can be extended by a factor of approximately 2–4. However, in several extreme cases, saturated absorption<sup>1</sup> occurs and the new technique also fails.

This study proposes to solve all the aforementioned conflicts by measuring SO<sub>2</sub> emissions through a multichannel gas analyzer with an optimized retrieval algorithm. This study is an extension of the study of Sun et al. (2013), but many optimizations in instrumentation and in the retrieval algorithm are performed as follows.

- a. We introduce two channels for SO<sub>2</sub> measurements to avoid the saturated absorption of SO<sub>2</sub>. One absorption channel, which lies on a relatively strong SO<sub>2</sub> absorption band, measures SO<sub>2</sub> in the lower concentration range, and another absorption channel, which lies on

<sup>1</sup>The absorbance no longer varies with gas concentrations because gas concentrations are beyond the upper limit of a channel.

a weaker absorption band, measures SO<sub>2</sub> in the higher concentration range. As a result, a good balance between sensitivity and measurement range can be obtained.

- b. The number of analysis channels is expanded from 8 to 11. More interfering gases are considered; thus, the system is robust during measurements of various industrial SO<sub>2</sub> emissions.
- c. Sun et al. (2013) established the interference equations depending on the interference conditions. The gas-to-gas interference is represented by a conventional constant factor if nonlinear absorption does not occur, whereas it is represented by a third polynomial if nonlinear absorption occurs. In addition, the H<sub>2</sub>O interference correction is included in the interference equations. In this study, all gas-to-gas interferences are represented by third polynomials. The H<sub>2</sub>O interference is corrected in a separate way, which shortens the calculation time when solving the interference equations. The optimized manner makes the system robust in linear and nonlinear conditions and thus can be easily adopted for other applications.

As a result, the optimized algorithm significantly improved the linearity restriction of the interference correction of the intended and interfering channels. Furthermore, the optimized algorithm significantly improved the measurement range by solving the saturated absorption problem and expanding accurate interference correction from the linear to nonlinear absorption regions.

In contrast to other well-established spectroscopic gas analyzers (e.g., differential optical absorption spectroscopy (DOAS) analyzer, Fourier transform infrared (FTIR) spectroscopy analyzer), the developed measurement technique presented in this study has the advantages of a simple setup, a wide measurement range for multi-gas analysis, low cost, and good durability. Furthermore, the developed measurement technique is more robust than the commercial multi-gas analyzer.

## 2 Instrument description

All experiments are performed with the compact multichannel gas analyzer prototype. The weight of the entire system is approximately 5 kg. Figure 1 shows the functional structure of this instrument. The light source (a globar) can be represented by a blackbody with a temperature of 1200 K (927 °C), covering infrared wavebands from 1 to 10 μm and with a maximum radiation wavelength  $\lambda_{\max}$  at 2.42 μm. Incoming light is reflected several times between three spherical mirrors ( $f = 396.3$  mm) to increase the light path length when it passes through the sample gas (resulting in 12 m optical path length within a white cell 60 cm long). The sam-

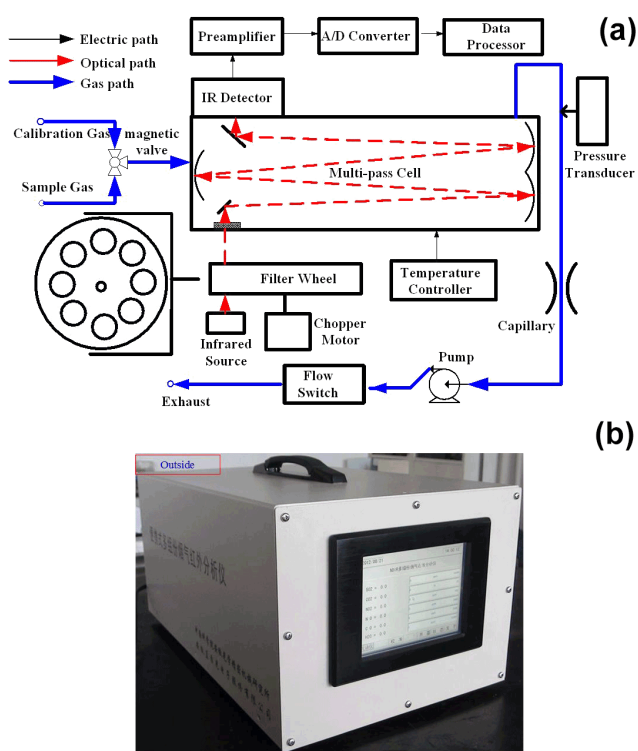


**Figure 1.** Layout of the experimental setup: (a) functional structure and (b) outside view.

ple cell is kept at 323 K (50 °C) with a temperature controller. The advantage of this prototype over the commercial gas analyzer is that it has a replaceable filter wheel that can be exchanged for other measurements. Suitable filter combinations allow the simultaneous measurement of a variety of gases, such as SO<sub>2</sub>, NO<sub>2</sub>, CH<sub>4</sub>, N<sub>2</sub>O, HC, H<sub>2</sub>O, CO<sub>2</sub>, CO, and NO (Sun et al., 2013). Our setup consists of four different filter wheels, namely, a four-channel filter wheel for atmospheric CO<sub>2</sub> and H<sub>2</sub>O measurements, a five-channel filter wheel for farmland/grassland/wetland CO<sub>2</sub> and CH<sub>4</sub> flux measurements, and an 8- or 11-channel filter wheel for industrial emissions' measurement. The corresponding signal sampling interval and data processing scenario can be adjusted according to the combination of filters.

For industrial emission measurements, the 8-channel or 11-channel filter wheel is selected depending on the type of interfering gases in the emissions. The filter wheel used in this study has 11 filter channels. Simultaneous measurements in 11 different wavelength channels are achieved with 11 different bandpass filters. One channel is used for system drift correction; two channels are used for SO<sub>2</sub> measurement; and the other eight channels are used to correct the interferences from NO, CO, CO<sub>2</sub>, NO<sub>2</sub>, CH<sub>4</sub>, HC, N<sub>2</sub>O, and H<sub>2</sub>O.

### 3 Filter parameters' calculation

The filter parameter and absorption characteristic of each channel should be determined before an instrument is constructed. We theoretically deduced the filter parameters of all channels based on the range requirements, Lambert–Beer's law, light path, and gas absorption parameters. We assumed that the instrument can reliably resolve optical signal attenuation between 5 and 95 % (an empirically estimated range based on the response performance of the detector); that is, the response range of the instrument lies between  $I_S = 0.05I_0$  and  $I_S = 0.95I_0$ . Therefore, the resolved absorbance range lies between 0.05129 and 2.9957 according to Lambert–Beer's law. The optical path length is a known constant ( $L = 1200$  cm), such that the measurement range of the instrument can be estimated when  $\alpha$  is derived. In this study,  $I_0$  and  $I_S$  represent the incident and emergent intensities, respectively.  $I_0$  and  $I_S$  can be obtained by the detector.  $\alpha$  (cm<sup>2</sup> molecule<sup>-1</sup>) is the total absorption coefficient of a gas within a specified wavelength interval  $\Delta\lambda$ , which can be calculated using a line-by-line integration method (Sparks, 1997; Martin and Michael, 1999; Rothman et al., 2005, 2009).

The absorption spectra of typical absorbers between 2 and 10  $\mu\text{m}$  obtained from the HITRAN database are shown in Fig. 2. Cross-absorptions interfering with each other are obvious. Three obvious absorption wavebands are observed within this region: at 4, 7.32, and 8.5  $\mu\text{m}$ . The line strengths of these three wavebands can be ranked as 7.32  $\mu\text{m} > 8.5 \mu\text{m} > 4 \mu\text{m}$ , with values of 10<sup>-19</sup>, 10<sup>-20</sup>, and 10<sup>-21</sup> cm molecule<sup>-1</sup>, respectively. Considering the radiation spectrum of the light source (the blue solid curve in Fig. 2b), we select the 7.32 and 4  $\mu\text{m}$  wavebands to measure the low and high concentration levels of SO<sub>2</sub> for a wide range from several ppmv to more than 10 000 ppmv. The 3.73  $\mu\text{m}$  band where SO<sub>2</sub> and the interference gases NO, CO, CO<sub>2</sub>, NO<sub>2</sub>, CH<sub>4</sub>, HC, N<sub>2</sub>O, and H<sub>2</sub>O show no or negligible absorption is selected as the reference channel. After the center wavelength of each filter channel is selected, its bandwidth can be determined through the following iterative scheme (Ehret et al., 1993; Bingham and Burton, 1984).

A starting wavelength interval  $\Delta\lambda$  with a small value is selected, and  $T$  and  $P$  are set as the temperature of the sample cell and one standard atmospheric pressure, respectively, i.e.,  $T = 323$  K and  $P = 101\,325$  Pa. Each line within this wavelength interval is described by a Voigt profile with the pressure and temperature dependence of the absorption line strengths and half-widths (Rothman et al., 2005, 2009). Thus, the total absorption coefficients of SO<sub>2</sub> at the three filter channels can be calculated numerically using line-by-line integration (Sparks, 1997; Martin and Michael, 1999). Then, the measurement range of each filter channel can be estimated from this total absorption coefficient and the aforementioned absorbance range. The uneven distribution of the light source and the response function of the detector within

a specified interval are neglected to simplify the line-by-line calculation. Furthermore, the transmission function  $t(\lambda)$  of a selected filter is approximated as a Gaussian function with a maximum transmission of 75 %. In this case,  $t(\lambda)$  can be expressed as follows:

$$t(\lambda) = \exp\left(-\left(\frac{\lambda - \lambda_0}{\Delta\lambda/4}\right)^2\right), \quad (1)$$

where  $\lambda_0$  represents the center wavelength. In this study,  $\Delta\lambda/4$  instead of the half-width of  $\Delta\lambda/2$  is used because the calculation results show that a Gaussian function of this form is closer to the actual transmission function of our filter (see Sect. 5.2).

If the measurement range estimated in step 1 meets the requirement, then the iteration is stopped and the bandwidth of this filter is determined. Otherwise,  $\Delta\lambda$  is increased by a small step  $\Delta$  and step 1 is repeated to calculate the next parameters.

Two important aspects should be considered for this iteration process.

- The determination of all filter parameters should consider the radiation distribution of the light source at each filter channel (see Fig. 2b). The bandwidth of a waveband near the maximum radiation wavelength  $\lambda_{\max}$  should be narrower than the bandwidth of a waveband further away from it. Filters are designed accordingly in a manner that ensures the detection of the optical signals of all channels with the same precision under a zero gas condition (e.g., 99.999 % N<sub>2</sub>). Therefore, the bandwidth of the 7.32  $\mu\text{m}$  (SO<sub>2</sub>(L)) waveband should be wider than that of the 4  $\mu\text{m}$  (SO<sub>2</sub>(H)) and 3.73  $\mu\text{m}$  (Ref) wavebands.
- A narrower reference filter channel means less interference from other gases and a better system. However, the optical signal of the reference filter channel should fulfill aspect (a).

The parameters of the SO<sub>2</sub>(L), SO<sub>2</sub>(H), and reference filters determined through the aforementioned method are listed in Table 1. The corresponding calculation results are listed in Table 2. The parameters of the other eight filters are obtained in a straightforward manner. Table 2 shows that the total absorption coefficients of SO<sub>2</sub> for the reference channel relative to the SO<sub>2</sub>(L) and SO<sub>2</sub>(H) channels are only  $6.1 \times 10^{-5}$  and  $2.76 \times 10^{-3}$ , respectively. The lower detection limit of the reference channel for SO<sub>2</sub> is 88 270.9 ppmv, which indicates that signal attenuation for this channel caused by SO<sub>2</sub> absorption (with concentration lower than 10 000 ppmv) can be neglected. Therefore, temporal variations of this channel are only caused by system drifts, and the reference channel can be used to correct the other channels (Jacob and Roy, 2012; Sun et al., 2013). The total absorption coefficient of SO<sub>2</sub> for the SO<sub>2</sub>(H) channel is only 2.02 % of that for the SO<sub>2</sub>(L) channel. If SO<sub>2</sub> is measured only through the SO<sub>2</sub>(L) channel, then a good lower

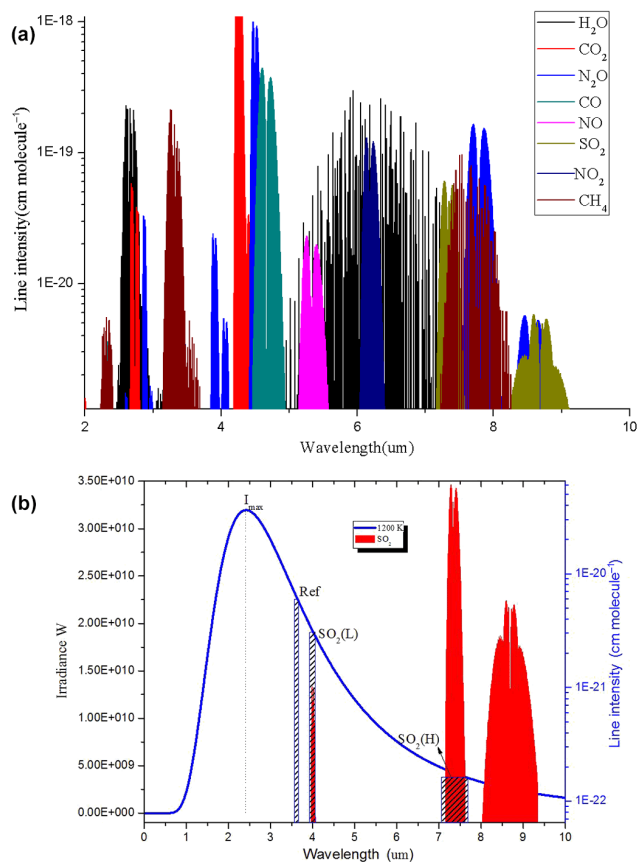


**Figure 2.** Absorption spectra of typical absorbers between 2 and 10  $\mu\text{m}$  obtained from the HITRAN database. The curves are in linear–log plots. **(a)** Absorption spectra of all typical absorbers. Obvious cross-absorptions with each other are shown. **(b)** Overview of the radiation distribution of the light source, the bandwidths of Ref, SO<sub>2</sub>(L) and SO<sub>2</sub>(H) filters, and the absorption spectra of SO<sub>2</sub>. Three obvious absorption wavebands at 4, 7.32, and 8.5  $\mu\text{m}$  are shown. Their line strengths ranked as 7.32  $\mu\text{m}$  > 8.5  $\mu\text{m}$  > 4  $\mu\text{m}$ , with values of  $10^{-19}$ ,  $10^{-20}$ , and  $10^{-21}$  cm molecule<sup>-1</sup>, respectively.

detection limit of 5.37 ppmv can be obtained. However, its upper detection limit is only 313.904 ppmv because of strong absorption. The upper detection limit of the SO<sub>2</sub>(H) channel is up to 14 224.6 ppmv. However, its lower detection limit is only 243.56 ppmv. Combining the SO<sub>2</sub>(L) and SO<sub>2</sub>(H) channels allows low and high concentrations of SO<sub>2</sub> to be measured from several ppmv to at least 10 000 ppmv. As a result, the saturated absorption of SO<sub>2</sub> is avoided, and the measurement range is improved significantly.

#### 4 Optimized concentration retrieval algorithm

Without correcting the cross-sensitivities caused by interfering gases, a gas analyzer is still incapable of resolving industrial SO<sub>2</sub> emissions over a wide range of variations even if

**Table 1.** Filter parameters: center wavelengths, bandwidths, and transmissions. The bandwidths of Ref, SO<sub>2</sub>(L), and SO<sub>2</sub>(H) filters are calculated using the iterative scheme described in the text. The transmissions of all filters are approximated by Gaussian functions with maximum transmission of 75 %.

| Channel no.            | No. 0            | No. 2                            | No. 3                            |
|------------------------|------------------|----------------------------------|----------------------------------|
| Filters                | Ref <sup>a</sup> | SO <sub>2</sub> (L) <sup>b</sup> | SO <sub>2</sub> (H) <sup>c</sup> |
| Center wavelength (μm) | 3.73             | 7.32                             | 4.00                             |
| Bandwidth (μm)         | 0.08             | 0.4                              | 0.1                              |
| Transmission (%)       | 75               | 75                               | 75                               |

<sup>a</sup> reference filter channel; <sup>b</sup> filter channel used to measure SO<sub>2</sub> for low concentration levels; <sup>c</sup> filter channel used to measure SO<sub>2</sub> for high concentration levels.

two absorption channels are used. The conventional method is only feasible for an application where the intended and interfering channels exhibit good linearity. In this section, an optimized SO<sub>2</sub> concentration retrieval algorithm is presented to make the instrument work well within the linear and non-linear ranges.

The optimized SO<sub>2</sub> concentration retrieval is briefly illustrated in Fig. 3. The retrieval algorithm (1) converts measurements values of all relevant channels into absorbance, (2) corrects for water vapor interference using the H<sub>2</sub>O channel, (3) makes cross-interference corrections using the interference equations, and (4) converts the cross-interference-corrected absorbance values into SO<sub>2</sub> concentrations. The nomenclature in Fig. 3 is listed in Table 3. We use an interference function instead of a constant factor to quantify gas-to-gas interference. All interference functions used in this study can be obtained through least squares fitting of a third polynomial (Sun et al., 2013). We now go through the steps shown in Fig. 3 in more detail.

1. The intensities of the other 10 analysis channels are divided by the reference channel to correct for hardware instability and are converted into absorbance. This step produces drift-compensated absorbance, representing the total absorption for each channel.
2. The H<sub>2</sub>O channel used for water vapor interference correction is designed to have a center wavelength of 2.59 μm and a bandwidth of 0.064 μm. The total absorption coefficients calculated in Sect. 3 show that the H<sub>2</sub>O channel has negligible response to other gases. Thus, water vapor interference can be easily corrected in this manner. In fact, (2) can be merged with (3) to result in 10 interference equations instead of 9 interference equations that must be solved simultaneously. The separation of the H<sub>2</sub>O channel facilitates the calculation of the interference equations and speeds up the concentration retrieval. This step produces water vapor interference-corrected absorbance, which represents the total absorption of each channel minus H<sub>2</sub>O absorption.

**(1) System drifts and/or hardware variations compensation:**

$$\begin{cases} \tau_t = \ln(I_0^t/I_0^{ref}) - \ln(I_S^t/I_S^{ref}) \\ t = 1 \sim 10 \end{cases}$$

**(2) Water vapor interference correction:**

$$\begin{cases} \tau'_t = \tau_t - k_{t1}(\tau_1) \\ t = 2 \sim 10 \end{cases}$$

**(3) Cross interference correction:**

$$\begin{cases} \tau'_2 = \tau'_2 + \sum_{i=3}^{10} k_{2i}(\tau'_i) \\ \tau'_3 = \tau'_3 + \sum_{i=2}^{10, i \neq 3} k_{3i}(\tau'_i) \\ \tau'_4 = \tau'_4 + \sum_{i=2}^{10, i \neq 4} k_{4i}(\tau'_i) \\ \tau'_5 = \tau'_5 + \sum_{i=2}^{10, i \neq 5} k_{5i}(\tau'_i) \\ \tau'_6 = \tau'_6 + \sum_{i=2}^{10, i \neq 6} k_{6i}(\tau'_i) \\ \tau'_7 = \tau'_7 + \sum_{i=2}^{10, i \neq 7} k_{7i}(\tau'_i) \\ \tau'_8 = \tau'_8 + \sum_{i=2}^{10, i \neq 8} k_{8i}(\tau'_i) \\ \tau'_9 = \tau'_9 + \sum_{i=2}^{10, i \neq 9} k_{9i}(\tau'_i) \\ \tau'_{10} = \tau'_{10} + \sum_{i=2}^9 k_{(10)i}(\tau'_i) \end{cases}$$

**(4) Gas concentration retrieval:**

$$\begin{cases} \tau'_2 \rightarrow Con.(SO_2) \\ \tau'_3 \rightarrow Con.(SO_2) \end{cases}$$

**Figure 3.** Four steps for SO<sub>2</sub> concentration retrieval. The instrument measures intensities of all channels. Measurement values are converted into absorbance and corrected for water vapor interference using the water vapor channel. Cross-interference corrections are performed using interference equations. Corrected absorbances are finally converted into SO<sub>2</sub> concentrations. See text for further details.

3. A set of interference equations is established with all fitted interference functions and the water vapor interference-corrected absorbance acquired in (2). The solution of these equations yields pure absorbance for each gas. The data processor can solve these equations iteratively because the absorbances are additive. In detail, the data processor sets up nine interference equations and creates a loop that “solves” these equations multiple times. The data processor starts the loop with

**Table 2.** Total absorption coefficients, lower and upper detection limits of Ref, SO<sub>2</sub>(L) and SO<sub>2</sub>(H) calculated using the parameters in Table 1.

| Channel no.         | Wavelength intervals (μm) | Total absorption coefficients (cm <sup>2</sup> molecule <sup>-1</sup> ) | Lower detection limits (ppmv) | Upper detection limits (ppmv) |
|---------------------|---------------------------|---|-------------------------------|-------------------------------|
| Ref                 | 3.65–3.81                 | $2.46113 \times 10^{-23}$   | 88270.9                       | $5.15537 \times 10^{+6}$      |
| SO <sub>2</sub> (L) | 6.92–7.72                 | $4.04201 \times 10^{-19}$   | 5.3747                        | 313.904                       |
| SO <sub>2</sub> (H) | 3.9–4.1                   | $8.91975 \times 10^{-21}$   | 243.556                       | 14224.6                       |

**Table 3.** The nomenclature in Fig. 3.

| Items                | Nomenclature  | Items   | Nomenclature  |
|----------------------|---|---|---|
| No. 1–10             | H <sub>2</sub> O, SO <sub>2</sub> (L), SO <sub>2</sub> (H), NO, NO <sub>2</sub> , CO, CO <sub>2</sub> , N <sub>2</sub> O, CH <sub>4</sub> , and HC channels, respectively | $\tau_t'' (t = 2-10)$                           | the cross-interference-corrected absorbance of channel no. <i>t</i>   |
| $\tau_t (t = 1-10)$  | drift compensated absorbance of channel no. <i>t</i>  | $k_{t1}(x) (t = 2-10)$                          | the interference function of H <sub>2</sub> O to channel no. <i>t</i> |
| $\tau_t' (t = 2-10)$ | water vapor interference-corrected absorbance of channel no. <i>t</i>   | $k_{ij}(x) (i, j = 2-10 \text{ and } i \neq j)$ | the interference function of gas <i>j</i> to channel no. <i>i</i>     |

the absorbance corrected for water vapor interference and uses the output of the loop as input for the next iteration. For example, for the first equation (for SO<sub>2</sub>), the data processor assumes that the total absorbance is generated by SO<sub>2</sub> (disregarding interferences) and that the absorbances of other gases are zero. With each pass through the loop, the data processor obtains a new absorbance that becomes available for the next iteration. In the second iteration, the data processor now has an estimated absorbance for each gas, such that it can apply the fitted interference functions and calculate the amount of interference that each gas would create in every channel. This estimation is only a rough approximation, but with each pass through the loop, the estimate improves and finally produces cross-interference-corrected absorbances, representing pure absorptions for each gas.

- The pure absorbances calculated in steps (1) to (3) are now used for concentration retrieval with the corresponding calibration curves. The flowchart of SO<sub>2</sub> retrieval is shown in Fig. 4. The concentration retrieval is attributed to the SO<sub>2</sub>(L) channel if the absorbance of this channel is lower than 1.5; otherwise, it is assigned to the SO<sub>2</sub>(H) channel. Calibration curves with four zero and/or span factors are used if the instrument has been zero- and/or span-calibrated. Otherwise, the default calibration curves are applied. The calibration curve fitting is discussed in Sect. 5.1.

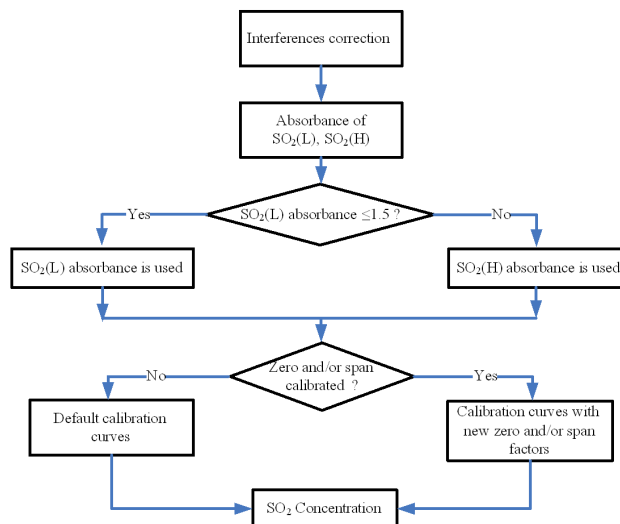


**Figure 4.** Flowchart of SO<sub>2</sub> concentration retrieval. The retrieval channel is chosen based on the interference-corrected absorbance of SO<sub>2</sub>(L). See text for further details.

## 5 Laboratory experiments and discussion

### 5.1 Calibration curves' fitting

The calibration curves of SO<sub>2</sub>(L) and SO<sub>2</sub>(H) can be obtained by assuming a parameterized (model) form of the concentration–absorbance relationship. The model parameters are determined from the least squares fit of the measured concentrations (Komhyr et al., 1983, 1989; Bjorck, 1996; Rao et al., 1999; Derek, 1968; Marcel and Zuberbuehler,

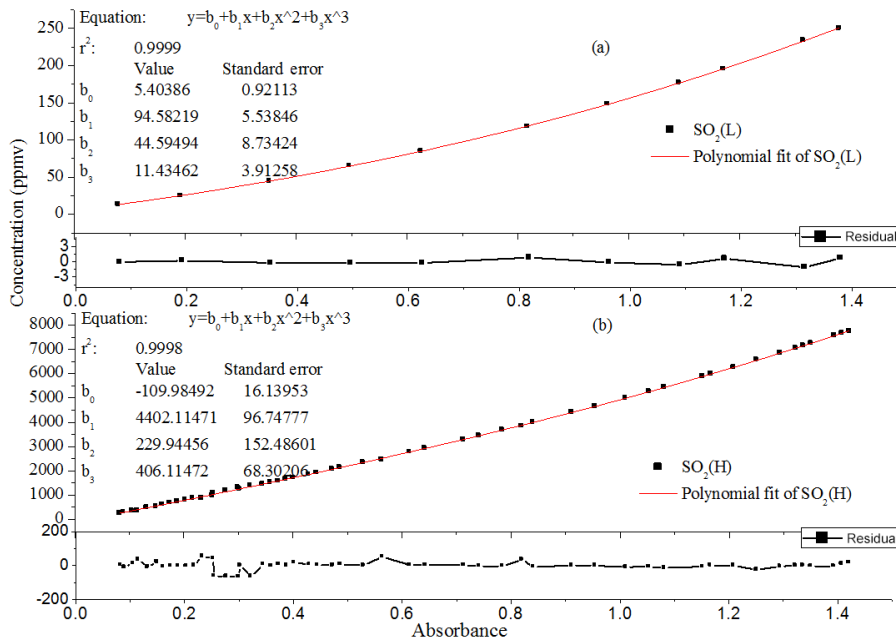


**Figure 5.** Calibration curves for the SO<sub>2</sub>(L) (a) and SO<sub>2</sub>(H) (b) as a result of least squares fitting using a third-order polynomial model.

1990). In principle, two different well-established fit models, namely, linear function and polynomial, are employed to obtain the calibration curves. In general, a gas analyzer has good linearity if gas concentrations lie within a specified range. In this case, a linear function model is used. Otherwise, a polynomial model is applied to obtain a relatively wider measurement range because a polynomial can effectively model the nonlinear absorption of a system compared with a linear function (Andre et al., 1985; Tan et al., 2008). In this study, a third-order polynomial model is used. The calibration experiments were conducted as follows. Different concentration levels of SO<sub>2</sub> generated by a gas generator were pumped into the sample cell. Each selected SO<sub>2</sub> level was stably maintained in the sample cell for the duration of 5 times the response time of the instrument to guarantee accurate optical intensity acquisitions. The data processor converts the intensities in the SO<sub>2</sub>(L) and SO<sub>2</sub>(H) channels into absorbance. The resulting data array ( $\tau_i^X, C_i$ ) for  $i = 1 - n$  concentration values  $C_i$  and the corresponding average absorbance values  $\tau_i^X$  of both channels  $X = \text{SO}_2(\text{L}), \text{SO}_2(\text{H})$  provide the input for calibration fit. SO<sub>2</sub> concentrations less than 280 ppmv are attributed to the SO<sub>2</sub>(L) channel, whereas concentrations greater than or equal to 280 ppmv are assigned to the SO<sub>2</sub>(H) channel. We selected the concentration value of 280 ppmv to separate the channels SO<sub>2</sub>(L) and SO<sub>2</sub>(H) because we observed a good balance between accuracy and linearity in this way. The boundary value 280 ppmv is an empirical result of multiple experiments. Figure 5a and b show the fitted calibration curves of the SO<sub>2</sub>(L) and SO<sub>2</sub>(H) channels, respectively. The fit parameters and their estimated errors, as well as the Pearson correlation coeffi-

cients, are included in both subfigures. Figure 5 shows that the SO<sub>2</sub>(L) and SO<sub>2</sub>(H) channels exhibit excellent fit results, with correlation coefficients of 0.9999 and 0.9998, respectively. The calibration curves of the two channels are expressed as Eqs. (2) and (3):

$$f_{\text{SO}_2(\text{L})}(\tau) = 5.40386 + 94.58219 \cdot \tau + 44.59494 \cdot \tau^2 + 11.43462 \cdot \tau^3 \quad (2)$$

$$f_{\text{SO}_2(\text{H})}(\tau) = -109.98492 + 4402.11471 \cdot \tau + 229.94456 \cdot \tau^2 + 406.11472 \cdot \tau^3. \quad (3)$$

Generally, calibration curves change with time because of instrument drift. Thus, zero and span calibrations must be performed and considered in the model for the calibration curve. These calibrations can be achieved by introducing zero and span factors such that the actual calibration curves of SO<sub>2</sub>(L) and SO<sub>2</sub>(H) become

$$f_{\text{SO}_2(\text{L})}^{\text{cal.}}(\tau) = d_0 \times f_{\text{SO}_2(\text{L})}(\tau) + j_0, \quad (4)$$

$$f_{\text{SO}_2(\text{H})}^{\text{cal.}}(\tau) = d_1 \times f_{\text{SO}_2(\text{H})}(\tau) + j_1, \quad (5)$$

where  $j_0$  and  $d_0$  denote the zero and span factors for the SO<sub>2</sub>(L) channel and  $j_1$  and  $d_1$  denote the zero and span factors for the SO<sub>2</sub>(H) channel. These correction factors are again obtained from measurements of calibration gases. Allan variance analysis of the measurement result was performed, and a compromise calibration cycle of 25 days was obtained for the SO<sub>2</sub>(L) and SO<sub>2</sub>(H) channels (Jacob and Roy, 2012; Sun et al., 2013).

## 5.2 Evaluation of the measurement range

Two approaches are commonly employed to estimate the detection limit because systematic errors are generally difficult to quantify (López and de Frutos, 1993; Sayed and Mohamed, 2010; Tyson et al., 1984). The first approach uses the concentration calculated for an absorbance equal to twice the standard deviation of the absorbance ( $2\sigma$  absorbance) under a zero gas (e.g., 99.999 % N<sub>2</sub>) condition to define the lower detection limit. The second approach has already been mentioned in Sect. 3; i.e., it assumes that an analyzer can only resolve optical signal attenuation above a critical threshold. Converting the optical attenuation into absorbance and employing the corresponding calibration curve for the concentration retrieval results in an alternative definition of the lower detection limit. We compare both approaches, considering 5 % signal attenuation as threshold for the second approach. Figure 6 shows an absorbance time series for the SO<sub>2</sub>(L) and SO<sub>2</sub>(H) channels under a zero gas (99.999 % N<sub>2</sub>) condition. Ten measurement cycles are averaged, resulting in a temporal resolution of approximately 4 s per reading. The statistical results of measurements taken for more than 10 h are listed in Table 4. For a  $2\sigma$  absorbance, the calibration curves for the SO<sub>2</sub>(L) and SO<sub>2</sub>(H) channels provide lower detection limits of 5.55 and 102.15 ppmv, respectively. Compared with the first approach, the second approach results in lower detection limits of 10.37 and 116.46 ppmv for the SO<sub>2</sub>(L) and SO<sub>2</sub>(H) channels, respectively. The upper detection limits for both channels are estimated through assumption, stating that 95 % of signal attenuation (absorbance of 2.9957) represents the upper limit of the analyzer. The values and channels are 997.23 ppmv (L) and 26 059.02 ppmv (H). Both of the estimation approaches show that the combination of the SO<sub>2</sub>(L) and SO<sub>2</sub>(H) channels is capable of measuring SO<sub>2</sub> concentrations from several ppmv to at least 10 000 ppmv, which is in good agreement with the estimations made in Sect. 3.

The differences between the measurement ranges estimated in this section and those in Sect. 3 can have various reasons. First, the estimations made in Sect. 3 and in this section are based on the linear Lambert–Beer’s law and third calibration curves (Eqs. 4 or 5), respectively, resulting in different detection limits. Second, the assumptions and approximations made during the numerical line-by-line integration result in errors such as those caused by approximating the transmission function for a Gaussian filter as well as those caused by neglecting the uneven distribution of the light source and the response function of the detector within a specified region. Figure 7 shows the actual transmissions of each filter designed according to Table 1. The actual transmissions of each filter obviously deviate from the assumed Gaussian shape. In addition to the dips in the real transmissions for the reference and SO<sub>2</sub>(H) channels, a notable shift of the center wavelength of the SO<sub>2</sub>(L) channel of approximately 0.03  $\mu$ m occurs. All these factors may re-

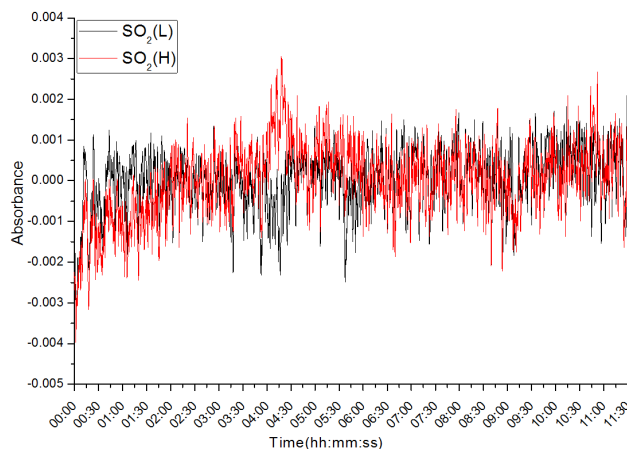


**Figure 6.** Absorbance time series for the SO<sub>2</sub>(L) and SO<sub>2</sub>(H) channel under a zero gas (99.999 % N<sub>2</sub>) condition. Sample data more than 10 h are included.

sult in differences between the calculated and actual values. Third, the signal attenuation assumed in the aforementioned estimations may contain a small portion of additional attenuation, e.g., attenuation due to scattering by dust, depositions on the filters, voltage fluctuations, and temperature drifts of the sample cell. These non-gas absorption processes are unavoidable and cannot be fully corrected by a reference channel.

In addition to the error sources previously mentioned, a principal problem occurs in assuming a 95 % signal attenuation for the estimation of the upper detection limit. The absorption spectrum within the full width of a filter consists of a large number of closely spaced lines. Between these lines, absorption does not occur, Lambert–Beer’s law does not apply, and the assumed 95 % attenuation of the total signal regardless of the gas concentration can be hardly reached in practice. For this reason, we set the upper detection limits of the SO<sub>2</sub>(L) and SO<sub>2</sub>(H) channels as 280 and 10 000 ppmv, respectively, although the estimated values are in fact higher. In addition, for this conservative estimate of the upper detection limit, the instrument features a better linearity for SO<sub>2</sub>.

## 5.3 Evaluation of the measurement accuracy

Gas mixtures (N<sub>2</sub>, H<sub>2</sub>O, CO<sub>2</sub>, CO, NO<sub>x</sub>, and SO<sub>2</sub>) with 15 different concentrations of SO<sub>2</sub> are pumped sequentially into the sample cell for analysis after the instrument has been zero- and span-calibrated. A total of 5 and 10 concentrations lie within the measurement range of the SO<sub>2</sub>(L) and SO<sub>2</sub>(H) channels, respectively. Gas mixtures are mixed in a manner that all the H<sub>2</sub>O, CO<sub>2</sub>, CO, and NO<sub>x</sub> channels exhibit nonlinear absorptions at least once within all the 15 measurements. The optimized concentration retrieval algorithm is embedded and the SO<sub>2</sub> measurement results and corresponding measurement errors are listed in Table 5. We define the measurement bias  $\Delta C$  and measurement error  $\gamma$  in Eq. (6):

**Table 4.** Statistical results for the absorbance time series in Fig. 6; the corresponding estimation results for measurement range are also included. Ten measurement cycles are averaged, resulting in a temporal resolution of approximately 4 s per reading.

| Channel no.         | Sample no. | Mean (-) <sup>a</sup>     | 1σ standard deviation (-) | Maximum (-) | Minimum (-) | LDL <sup>b</sup> (ppmv) | UDL <sup>c</sup> (ppmv) |
|---------------------|------------|---------------------------|---------------------------|-------------|-------------|-------------------------|-------------------------|
| SO <sub>2</sub> (L) | 8275       | $-5.76798 \times 10^{-7}$ | $7.59723 \times 10^{-4}$  | 0.00209     | -0.00324    | 5.54768                 | 997.23                  |
| SO <sub>2</sub> (H) | 8275       | $2.98175 \times 10^{-6}$  | $8.90672 \times 10^{-4}$  | 0.00306     | -0.00397    | 102.14842               | 26059.02                |

<sup>a</sup> absorbance; <sup>b</sup> lower detection limit; <sup>c</sup> upper detection limit.

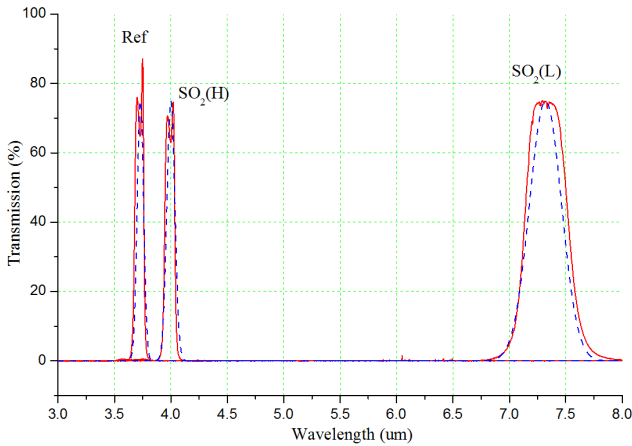


**Figure 7.** Transmissions of the filters in Table 1. The red solid lines are actual transmission functions and the blue dotted lines are corresponding Gaussian functions assumed in Sect. 3.

$$\gamma = \frac{\Delta C}{C_T} \quad (6)$$

$$\Delta C = C_M - C_T,$$

where  $C_T$  and  $C_M$  represent the true and measured concentrations. Table 5 shows that measurement errors in most cases are less than 2%. Figure 8 shows the correlation between the measured and true concentrations. An excellent correlation coefficient  $r^2$  of 0.99977 is obtained (López and de Frutos, 1993; Sayed and Mohamed, 2010; Tyson et al., 1984). Measurement biases and measurement errors are shown in Fig. 9. For the same channel, measurement biases for low concentrations are obviously less than those for high concentrations. A possible reason is that high concentrations are relatively more influenced by span calibration error. Furthermore, measurement biases of the SO<sub>2</sub>(H) channel are obviously larger than those of the SO<sub>2</sub>(L) channel because the SO<sub>2</sub>(H) channel is less sensitive to signal attenuation than the SO<sub>2</sub>(L) channel. Thus, system noise has a relatively more significant influence on the SO<sub>2</sub>(H) channel than on the SO<sub>2</sub>(L) channel. However, both channels show that measurement errors for high concentrations are obviously smaller than those for low concentrations because of the larger denominators that they are divided by (see Eq. 6).

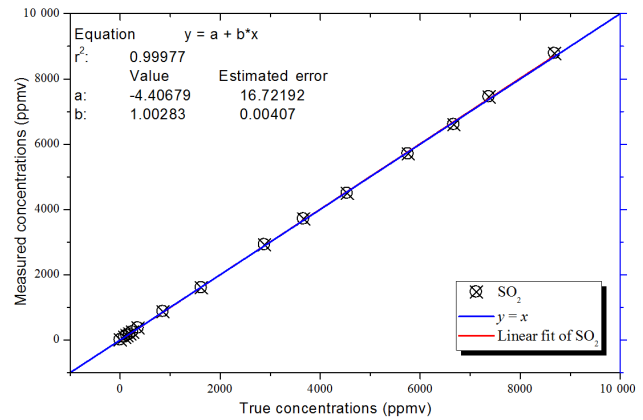


**Figure 8.** Linear correlation between measured and true concentrations. An excellent Pearson correlation coefficient  $r^2$  of 0.99977 is obtained.

### 5.4 Comparison between the conventional and optimized methods

We use different combinations of SO<sub>2</sub>, H<sub>2</sub>O, and N<sub>2</sub> gases to simulate the linear and nonlinear absorptions in the H<sub>2</sub>O channel. The SO<sub>2</sub> concentration was kept at a constant, whereas the H<sub>2</sub>O concentration was filled from low to high level. This manner allows for a gradual variation of the H<sub>2</sub>O channel from the linear range to the nonlinear range of absorption. Values of 243 and 6672 ppmv were selected as the references for the SO<sub>2</sub>(L) and SO<sub>2</sub>(H), respectively. Figure 10 shows the comparison of the relative measurement errors between the conventional and optimized retrieval algorithm. The conventional and optimized algorithms work well if H<sub>2</sub>O absorption lies within a linear range and all relative measurement errors are less than 2%. However, the optimized method works significantly better than the conventional method if nonlinear absorption occurs. In this case, nonlinear absorption has a negligible influence on the optimized method, whereas measurement errors using the conventional method deteriorate abruptly. In addition, the H<sub>2</sub>O nonlinear absorption has a more significant influence on the SO<sub>2</sub>(L) channel than on the SO<sub>2</sub>(H) channel because H<sub>2</sub>O exhibits stronger interference in the SO<sub>2</sub>(L) channel than in the SO<sub>2</sub>(H) channel.

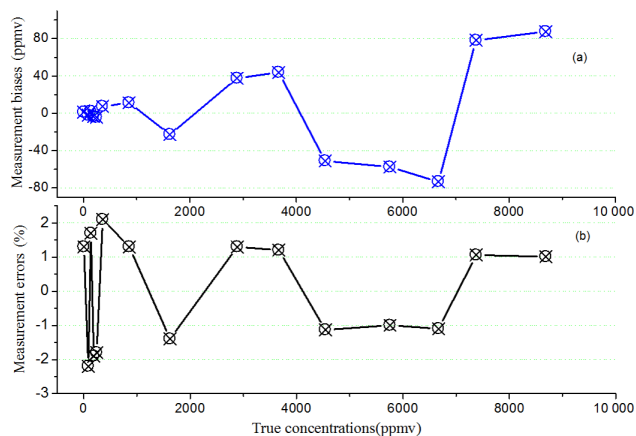


**Figure 9.** Comparison of measurement bias (a) and measurement errors (b) for all concentrations in the laboratory experiment. The measurement bias obviously increases with increasing concentrations. Measurement errors for high concentrations are smaller than those for low concentrations.

**Table 5.** SO<sub>2</sub> measurement results and corresponding measurement errors. Gas mixtures (H<sub>2</sub>O, CO<sub>2</sub>, CO, NO<sub>x</sub>, and SO<sub>2</sub>) with 15 different concentrations of SO<sub>2</sub> are measured in sequence; 5 and 10 concentrations of these gases lie within the measurement range of the SO<sub>2</sub>(L) and SO<sub>2</sub>(H) channel, respectively.

| No. | True concentration (ppmv) | Measured concentration (ppmv) | Measurement biases $\Delta C$ (ppmv) | Measurement errors $\gamma$ (%) |
|-----|---------------------------|-------------------------------|--------------------------------------|---------------------------------|
| 0   | 0                         | 1.3                           | +1.3                                 | +1.3                            |
| 1   | 86                        | 84.1                          | -1.9                                 | -2.2                            |
| 2   | 132                       | 134.3                         | +2.3                                 | +1.7                            |
| 3   | 187                       | 184.4                         | -3.6                                 | -1.9                            |
| 4   | 243                       | 238.6                         | -4.4                                 | -1.8                            |
| 5   | 356                       | 363.5                         | +7.5                                 | +2.1                            |
| 6   | 855                       | 866.1                         | +11.1                                | +1.3                            |
| 7   | 1623                      | 1600.3                        | -22.7                                | -1.4                            |
| 8   | 2884                      | 2921.5                        | +37.5                                | +1.3                            |
| 9   | 3667                      | 3711                          | +44                                  | +1.2                            |
| 10  | 4543                      | 4492                          | -51                                  | -1.13                           |
| 11  | 5758                      | 5700.4                        | -57.6                                | -1.0                            |
| 12  | 6672                      | 6598.6                        | -73.4                                | -1.1                            |
| 13  | 7376                      | 7454.2                        | +78.2                                | +1.06                           |
| 14  | 8688                      | 8775.7                        | +87.7                                | +1.01                           |

We performed similar experiments to simulate the linear and nonlinear absorptions in other channels, and the superiority of the optimized method was also concluded from the comparisons.

## 6 Field campaigns

The multichannel analyzer has been used to monitor the SO<sub>2</sub> emissions of three factories as shown in Fig. 11. These factories are located in the suburbs of the city of Tongling (south of Hefei, Anhui province) in central China, where

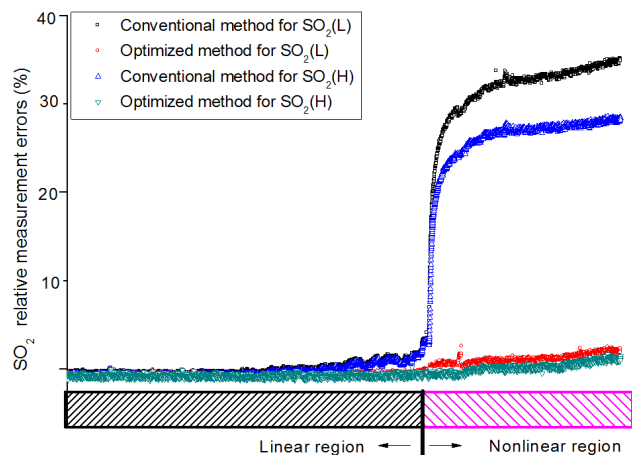


**Figure 10.** Comparison between the conventional and the optimized retrieval algorithm. H<sub>2</sub>O absorption varied gradually from linear region to nonlinear region.

they form a triangle near the Yangtze River. All these factories, namely, Fuxin steel plant (30.58° N, 118.1° E), Wan power plant (30.52° N, 117.46° E), and Shangfeng cement plant (30.48° N, 117.48° E) are equipped with commercial DOAS analyzers that measure SO<sub>2</sub> emissions before and/or after desulfurization. All DOAS analyzers can accurately resolve SO<sub>2</sub> emissions in these three factories (<http://www.ldchina.cn/NNews.asp?id=92>). Thus, their measurements are taken as reference in the subsequent comparisons. The three factories provide different interfering gas types and concentration levels. Fuxin steel plant exhibits the most interference from CO and CO<sub>2</sub>. The interference in Wan power plant mainly comes from CO and NO<sub>x</sub>, whereas the interference in Shangfeng cement plant comes from H<sub>2</sub>O, CO, and CO<sub>2</sub>. CO in Fuxin steel plant, NO<sub>x</sub> in Wan power plant, and H<sub>2</sub>O or CO<sub>2</sub> in Shangfeng cement plant occasionally exhibit nonlinear absorptions. The accuracy level of all measurements can be used to evaluate the performance of interference corrections within the multichannel analyzer.

We conducted two field campaigns in July 2011 and March 2012. The first campaign was conducted over 3 days from 6 to 8 July 2011 only in the Fuxin steel plant. The second campaign lasted 10 days from 18 to 27 March 2012 sequentially performed in the Wan power plant and Shangfeng cement plant. The multichannel analyzer was used to measure SO<sub>2</sub> emissions before desulfurization in the Fuxin steel plant and Wan power plant, as well as SO<sub>2</sub> emissions after desulfurization in the Shangfeng cement plant. All measurements were performed simultaneously with DOAS analyzers. The setup for the stack measurements is shown in Fig. 12. The pretreated samples were pumped into the reference analyzer (the DOAS analyzer) and the multichannel analyzer through a four-port distribution chamber. The pretreatment system was used to remove dusts and liquids. The sample system blew back once an hour to prevent the dust

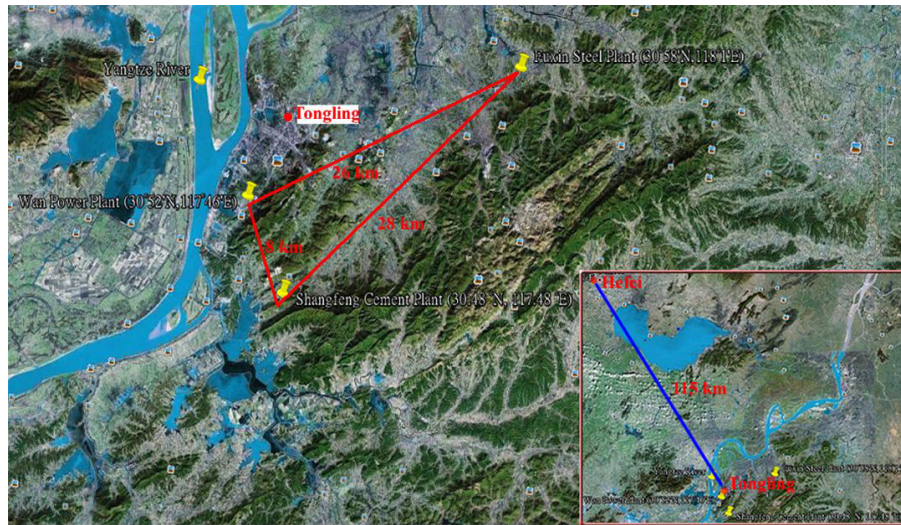


**Figure 11.** The location of the Fuxin steel plant (30.58° N, 118.1° E), the Wan power plant (30.52° N, 117.46° E), and the Shangfeng cement plant (30.48° N, 117.48° E). The three factories form a triangle near the Yangtze River, and all are located in the suburbs of the city of Tongling (south of Hefei, Anhui province) in central China.

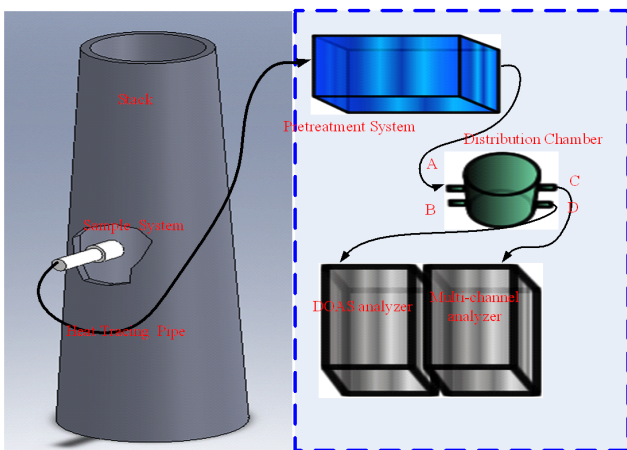


**Figure 12.** Setup for stack measurements with the multichannel analyzer and a DOAS analyzer. A detailed description of a similar setup can be found in Sun et al. (2013).

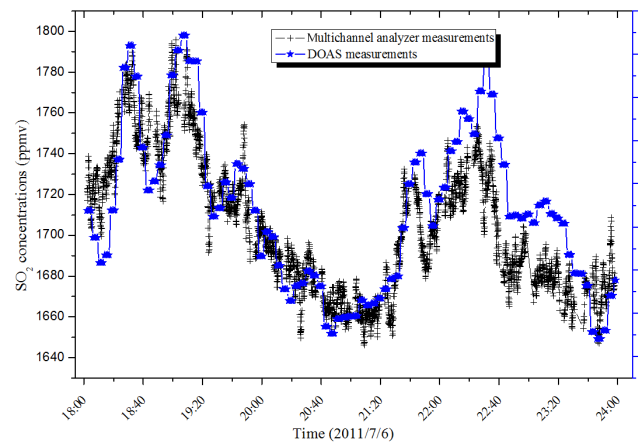


**Figure 13.** SO<sub>2</sub> concentration series of Fuxin steel plant measured with the DOAS analyzer and the multichannel analyzer on 6 July 2011. Measurements acquired during the blowback period are removed.

filter from being jammed (this process is called blowback). The multichannel analyzer was zero- and span-calibrated before the experiments. Further details can be found in Sun et al. (2013).

Figure 13 shows the SO<sub>2</sub> time series of Fuxin steel plant measured with the DOAS analyzer and the multichannel analyzer on 6 July 2011. Measurements acquired during the blowback period were removed. The SO<sub>2</sub> measurements of the two analyzers exhibited similar trends. Overall, SO<sub>2</sub> concentrations were higher than 1000 ppmv and were mainly concentrated between 1600 and 1800 ppmv. Figure 14 shows the corresponding correlation between the two analyzers after the outliers (measurements acquired during the blowback

period) were removed. The correlation is quite good with  $r^2 = 0.93218$ .

Figure 15 shows the SO<sub>2</sub> time series of Wan power plant measured with the DOAS analyzer and the multichannel analyzer from 15:08 LT on 19 March 2012 to 14:38 LT on 22 March 2012. Both analyzers acquired measurements once a minute, resulting in at least 4000 reliable measurements. For illustration, the measurements acquired during the blowback period were included, visible as outliers (sharp dips) in regular time intervals in Fig. 15. During the blowback period, gas samples pumped into the two analyzers were a mixture of emission residuals and ambient air, causing measured concentrations to decline abruptly. The outliers measured with

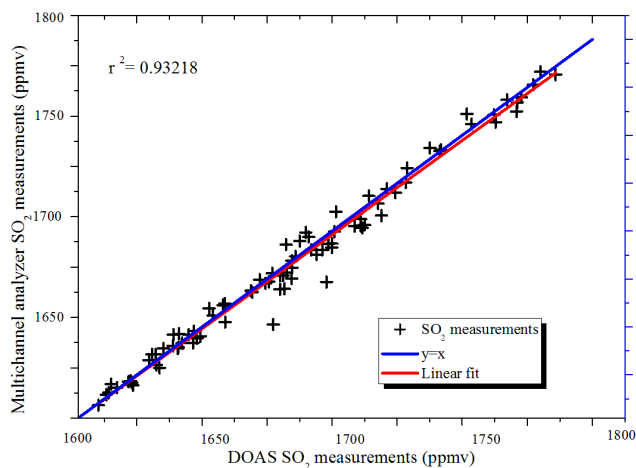


**Figure 14.** Correlation between SO<sub>2</sub> concentrations measured with the DOAS analyzer and the multichannel analyzer on 6 July 2012 at the Fuxin steel plant. Outliers during the blowback period are removed.

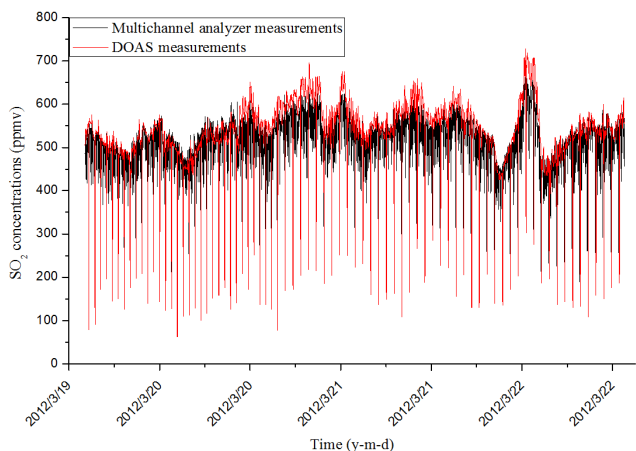


**Figure 15.** SO<sub>2</sub> concentrations time series of Wan power plant measured with the DOAS analyzer and the multichannel analyzer during 18 to 27 March 2012. Measurements acquired during the blowback period are included, appearing as sharp dips of the concentration at fixed intervals.

the DOAS analyzer appeared sharper than those measured with the multichannel analyzer because the volume of the sample cell in the multichannel analyzer is larger than that in the DOAS analyzer.

The trends of both concentration time series also agree well if outliers are discarded (outliers can be removed easily because blowback procedures are performed at fixed intervals). Figure 16 shows the correlation between the two analyzers after the outliers are removed. A reasonable correlation with  $r^2 = 0.86$  can be observed for both types of measurements. The dense region within the green box represents SO<sub>2</sub> concentrations appearing with the highest frequency. Corresponding concentrations range from 450 to 600 ppmv.

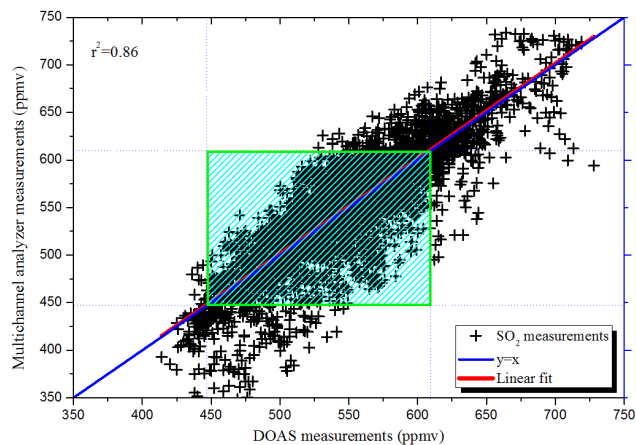


**Figure 16.** Correlation between the DOAS analyzer and the multichannel analyzer for the time series shown in Fig. 15 after outliers were removed. The green box represents SO<sub>2</sub> concentrations that appeared with the highest frequency.

Figure 17 shows the times series of the hourly averaged SO<sub>2</sub> concentrations at Shangfeng cement plant measured with the DOAS analyzer and the multichannel analyzer from 18 to 27 March 2012. The measurements acquired during the blowback period were removed again. Both analyzers show a similar trend. SO<sub>2</sub> concentrations in most cases were less than 300 ppmv and were mainly between 150 and 300 ppmv. Their correlation is illustrated in Fig. 18 ( $r^2 = 0.89$ ). The green box has the same meaning as that in Fig. 16. Another continuous DOAS measurement shows that the SO<sub>2</sub> concentrations of this factory before desulfurization are usually approximately 600 to 900 ppmv, which are approximately 3 times the concentrations measured during this field campaign.

Figures 13 and 17 show some discrepancies between the two instruments at certain time intervals. These discrepancies are most likely related to surrounding vibrations such as those caused by certain production processes or a nearby air compressor operating occasionally to obtain sufficient compressed air for the blowback system. These vibrations interfere with both measurements by causing a certain disturbance to the optical or mechanical parts of both instruments. In Fuxin steel plant (Fig. 13) and Shangfeng cement plant (Fig. 17), all instruments were placed in a shabby mini-house built at approximately 15 m in height and were only connected to the stack. Meanwhile, in Wan power plant (Fig. 15), all instruments were placed in a rugged house on the ground and were not connected to the stack. More vibrations were observed in the instruments shown in Figs. 13 and 17 than those shown in Fig. 15. Therefore, Fig. 15 exhibits fewer discrepancies than Figs. 13 and 17. Notably, good agreement between the two analyzers in the three factories shows that the multichannel analyzer is capable of monitoring SO<sub>2</sub> emissions in various industrial applications.

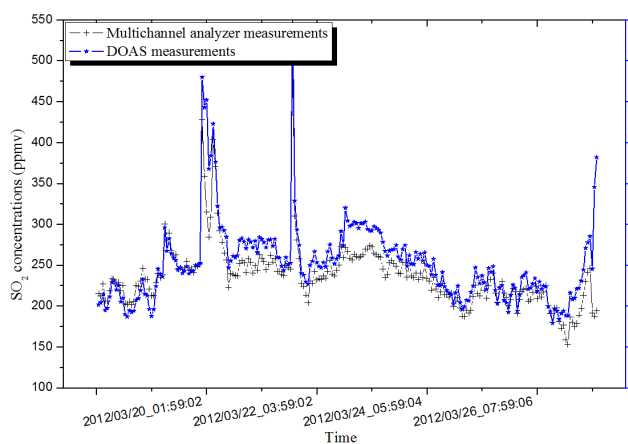


**Figure 17.** Time series of hourly averaged SO<sub>2</sub> concentrations measured with the DOAS analyzer and the multichannel analyzer at the Shangfeng cement plant.

## 7 Conclusions

Industrial SO<sub>2</sub> emissions vary over a wide range and are embedded in exhausts composed of a mixture of different gases, which might affect the measurements of SO<sub>2</sub> in the infrared spectral region because of their interfering absorptions. We design a multichannel gas analyzer with an optimized retrieval algorithm to solve these problems. The multichannel gas analyzer measures the optical absorption of 11 wavelength channels simultaneously. We determined the filter parameters for all channels based on the measurement range requirements, a line-by-line calculation method, and an iterative scheme. Gaussian transmission functions for all filters are assumed. The influence of temperature and pressure on the absorption line strengths and line shape functions are considered precisely in the data analysis. An optimized retrieval algorithm is developed to retrieve SO<sub>2</sub> concentration. The algorithm uses a third polynomial instead of a constant factor to quantify gas-to-gas interference. The developed technique solved the linearity restriction of conventional interference correction of the intended and interfering channels. As a result, the interference correction can be extended to the nonlinear range. A good balance between sensitivity and measurement range was obtained, and SO<sub>2</sub> concentrations ranging from approximately 5 to 10 000 ppmv can be detected with excellent accuracy. Laboratory and field experiments are performed to evaluate the performance of the developed retrieval algorithm within this multichannel gas analyzer. The results show that the multichannel gas analyzer is a robust solution for SO<sub>2</sub> emission monitoring in industrial facilities. This measurement technique can potentially be applied to measurements of other gases, such as CO<sub>2</sub>, H<sub>2</sub>O, and NO<sub>2</sub>, that feature a wide range of concentration variation.

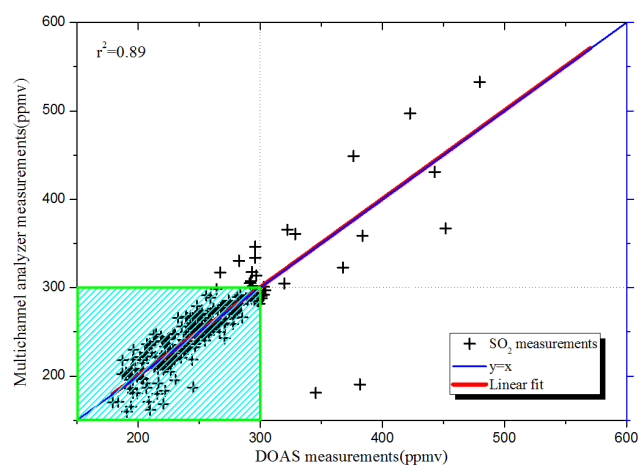


**Figure 18.** Correlation between the two analyzers for the time series of Fig. 17. The green box again represents SO<sub>2</sub> concentrations appearing with the highest frequency.

*Acknowledgements.* This work is jointly supported by Anhui Province Natural Science Foundation of China (grant no. 1308085QF124, no. 1608085MD79), the National Science Foundation of China (grants no. 41530644, no. 41571130023, no. 41275038, no. 91544212 and no. 41575021), the National Key Technology R&D Program of China (2014BAC22B00), the National High Technology Research and Development Program of China (2014AA06A508, 2014AA06A511), the Scientific and Technological Project of Anhui Province (1301022083), and the Special Project of Environmental Nonprofit Industry Research China (201409006). We thank Fuxin steel plant, Wan power plant, and Shangfeng cement plant for access to the field sites. We would like to thank our colleague Y. Zhen for the source code of the Voigt profile calculation software which formed the basis of the total absorption coefficients' calculation program in this study. The DOAS measurements are all provided by Landun Environmental Instruments, Inc.

Edited by: M. von Hobe

## References

- Andre, G., Gerard, F., and Pierre, C.: Gas concentration measurement by spectral correlation: rejection of interfering species, *Appl. Optics*, 14, 2127–2132, 1985.
- Bingham, D. and Burton, C. H.: Analysis of multi-component gas mixtures by correlation of infrared spectra, *Appl. Spectrosc.*, 5, 705–709, 1984.
- Bjorck, A.: *Numerical Methods for Least Squares Problems*, SIAM, available at: <http://www.ec-securehost.com/SIAM/ot51.html> (last access: 2 March 2013), 1996.
- Chan, C. K. and Yao, X.: Air pollution in mega cities in china, *Atmos. Environ.*, 42, 1–42, 2008.
- Derek, Y.: Least squares fitting of a straight line with correlated errors, *Earth Planet. Sc. Lett.*, 5, 320–324, 1968.

- Dirk, A., Gaston, E. M., Shrikrishna, H. N., and Robert, F. M.: Gas Analyzer System, US Pat US/2009/0213380 A1, 27 August 2009.
- Ehret, G., Kiemle, C., Renger, W., and Simmet, G.: Airborne remote sensing of tropospheric water vapor with a near infrared differential absorption lidar system, *Appl. Optics*, 24, 4534–4549, 1993.
- EPER: European Pollutant Emission Register 2004, available at: <http://www.eea.europa.eu/> (last access: 1 February 2012), 2004.
- European Commission: 2007/589/EC, establishing guidelines for the monitoring and reporting of greenhouse gas emissions pursuant to Directive 2003/87/EC of the European Parliament and of the Council, *Official Journal of the European Union*, 2210, 2007.
- Evans, S., Deery, S., and Bionda, J.: How Reliable are GHG Combustion Calculations and Emission Factors, Presented at the CEM 2009 Conference, 23–25 September 2009, Milan, Italy, 2210, 2240, 2009.
- Gary, K.: An open path H<sub>2</sub>O = CO<sub>2</sub> gas analyzer for eddy correlation systems: theory and design, *Spectrochim. Acta A*, 58, 2373–2388, 2002.
- Harold, S. L., Satoru, S., Louis, J. D., and Alberto, M. G.: Non-Dispersive Infrared Gas Analyzer with Interfering Correction, US Pat 5886348, 23 March 1999.
- Herget, W. F., Jahnke, J. A., Burch, D. E., and Gryvnak, D. A.: Infrared gas filter correlation instrument for in situ measurement of gaseous pollutant concentrations, *Appl. Optics*, 15, 1222–1225, 1976.
- Jacob, Y. W. and Roy, L. A.: Non-dispersive infrared gas measurement, IFSA Publishing, 2, 4–69, 2012.
- Komhyr, W. D., Waterman, L. S., and Taylor, W. R.: Semi-automatic non-dispersive infrared analyzer apparatus for CO<sub>2</sub> air sample analyses, *J. Geophys. Res.*, 88, 1315–1322, doi:10.1029/JC088iC02p01315, 1983.
- Komhyr, W. D., Harris, T. B., Waterman, L. S., Chin, J. F. S., and Thoning, K. W.: Atmospheric carbon dioxide at Mauna Loa Observatory: 1. NOAA global monitoring for climatic change measurements with a non-dispersive infrared analyzer, *J. Geophys. Res.-Atmos.*, 94, 7–29, 1989.
- Lambrecht, A.: Quantum cascade lasers, systems, and applications, in: Europe, Quantum Sensing and Nanophotonic Devices II, edited by: Razeghi, M. and Brown, G. J., *Proceedings of SPIE Vol. 5732*, SPIE, Bellingham, WA, doi:10.1117/12.606470, 2–7 November 2005.
- Liu, C., Beirle, S., Butler, T., Liu, J., Hoor, P., Jöckel, P., Penning de Vries, M., Pozzer, A., Frankenberg, C., Lawrence, M. G., Lelieveld, J., Platt, U., and Wagner, T.: Application of SCIAMACHY and MOPITT CO total column measurements to evaluate model results over biomass burning regions and Eastern China, *Atmos. Chem. Phys.*, 11, 6083–6114, doi:10.5194/acp-11-6083-2011, 2011.
- López, F. and de Frutos, J.: Multi-spectral interference filters and their application to the design of compact non-dispersive infrared gas analyzers for pollution control, *Sensor. Actuat. A-Phys.*, 37, 502–506, 1993.
- Marcel, M. and Zuberbuehler, A. D.: Nonlinear least-squares fitting of multivariate absorption data, *Anal. Chem.*, 62, 2220–2224, 1990.
- Mark, A. M., Chris, W. B., and Donald, S. L.: Nonlinear multi-component analysis by infrared spectrophotometry, *Anal. Chem.*, 11, 1694–1703, 1983.
- Martin, K. and Michael, H.: Efficient line-by-line calculation of absorption coefficients, *J. Quant. Spectrosc. Ra.*, 63, 97–114, 1999.
- Mauri, A. R., Llobat, M., and Adria, D.: Detection and correction of interferences in spectroscopy techniques, *Anal. Chim. Acta*, 426, 135–146, 2001.
- Rao, C. R., Toutenburg, H., Fieger, A., Heumann, C., Nittner, T., and Scheid, S.: *Linear Models: Least Squares and Alternatives*, Springer Series in Statistics, Springer-Verlag New York, Inc., New York, 1999.
- Rothman, L., Jacquemart, D., Barbe, A., Benner, D. C., Birk, M., Brown, L., Carleer Jr, M. C. C., Chance, K., Coudert, L., Dana, V., Devi, V., Flaud, J.-M., Gamache, R., Goldman, A., Hartmann, J.-M., Jucks, K., Makim, A., Mandin, J.-Y., Massie, S., Orphal, J., Perrin, A., Rinsland, C., Smith, M., Tennyson, J., Tolchenov, R., Toth, R., Auwera, J. V., Varanasi, P., and Wagner, G.: The HITRAN 2004 molecular spectroscopic database, *J. Quant. Spectrosc. Ra.*, 96, 139–204, doi:10.1016/j.jqsrt.2004.10.008, 2005.
- Rothman, L., Gordon, I., Barbe, A., Benner, D., Bernath, P., Birk, M., Boudon, V., Brown, L., Campargue, A., Champion, J.-P., Chance, K., Coudert, L., Dana, V., Devi, V., Fally, S., Flaud, J.-M., Gamache, R., 5 Goldman, A., Jacquemart, D., Kleiner, I., Lacome, N., Lafferty, W., Mandin, J.-Y., Massie, S., Mikhailenko, S., Miller, C., Moazzen-Ahmadi, N., Naumenko, O., Nikitin, A., Orphal, J., Perevalov, V., Perrin, A., Predoi-Cross, A., Rinsland, C., Rotger, M., Simeckova, M., Smith, M., Sung, K., Tashkun, S., Tennyson, J., Toth, R., Vandaele, A., and Auwera, J. V.: The HITRAN 2008 molecular spectroscopic database, *J. Quant. Spectrosc. Ra.*, 110, 533–572, doi:10.1016/j.jqsrt.2009.02.013, 2009.
- Sayed, A. M. M. and Mohamed, H. A.: Gas analyzer for continuous monitoring of carbon dioxide in gas streams, *Sensor. Actuator*, 145, 398–404, 2010.
- Sparks, L.: Efficient line-by-line calculation of absorption coefficients, *J. Quant. Spectrosc. Ra.*, 57, 31–50, 1997.
- Sun, Y. W., Liu, C., Chan, K. L., Xie, P. H., Liu, W. Q., Zeng, Y., Wang, S. M., Huang, S. H., Chen, J., Wang, Y. P., and Si, F. Q.: Stack emission monitoring using non-dispersive infrared spectroscopy with an optimized nonlinear absorption cross interference correction algorithm, *Atmos. Meas. Tech.*, 6, 1993–2005, doi:10.5194/amt-6-1993-2013, 2013.
- Tan, Q. L., Zhang, W. D., Xue, C. Y., Xiong, J. J., Ma, Y. C., and Wen, F.: Design of mini-multi-gas monitoring system based on IR absorption, *Opt. Laser. Technol.*, 40, 703–710, 2008.
- Terje, B.: Impact of increased anthropogenic emission in Asia on troposphere ozone and climate, *Tellus*, 3, 251–254, 1996.
- Tyson, L., Ling, Y. C., and Charles, K. M.: Simultaneous multi-component quantitative analysis by infrared absorption spectroscopy, *Appl. Spectrosc.*, 5, 38–56, 1984.
- Zu, S. F.: Present status and developing countermeasure of tail exhaust gas measurement of China motor vehicle, *Auto. Ind. Res.*, 4, 25–28, 2002.